Geometrical matching and its influence on the melting transition of confined vortices in a mesoscopic triangle of $Bi_2Sr_2CaCu_2O_{8+y}$ superconductor

S. Ooi, M. Tachiki, T. Mochiku, K. Komori, K. Hirata, and S. Arisawa

National Institute for Materials Science, 1-2-1 Sengen, Tsukuba 305-0047, Japan

To study the melting transition of a vortex crystal (or cluster) consisting of a small number of vortices confined in a mesoscopic-scale superconductor, c-axis magnetoresistance in the highly anisotropic high-T_c superconductor $Bi_2Sr_2CaCu_2O_{8+y}$ (Bi2212) has been measured using a triangle-shaped stack of intrinsic Josephson junctions, which was trimmed out from a single-crystal flake of Bi2212 via a double-sided etching process using a focused ion beam. We observed oscillations of the melting transition line, in which the oscillating part of the melting temperature has sharp peaks when the number of vortices N exactly coincides with the triangular number $n(n + 1)/2$ (n is an integer number), at least for $N < 50$. This is in contrast to the case of square shapes where the enhancements appeared as broad peaks around $N = n^2$. Furthermore, the field ranges of the N-vortex state expand at the triangular numbers of N, suggesting that the triangular number of vortices has a more stable configuration than the others. Numerical studies on the configuration of vortices in a triangle shape show that geometrical matching with no defect structures is realized at the triangular numbers, whereas an edge dislocation often appears in the other nonmatching cases. The degree of suppression of the melting temperatures at nonmatching numbers is reasonably consistent with the value estimated from the increase in free energy with the introduction of an edge dislocation.

I. INTRODUCTION

In general, spatially confined interacting elements self-organize various structures depending on the functional form of interaction, the boundary condition or potential for the confinement, the dimensionality, quantum or classical behavior, etc. For instance, electrons in an atom have a shell structure in which they are confined in a three-dimensional spherically symmetric Coulomb potential of a positively charged atomic nucleus. In this case, the quantum nature of electrons is essential to understanding the periodicity with an increase in the atomic number, i.e., the periodic table of elements. Regarding two-dimensionally confined macroscopic elements, spatial arrangements such as shell structures have been observed in various systems: vortices in superconductors [1], superfluid He [2] and Bose-Einstein condensate of cold atoms [3,4], dusty plasma [5], magnetized colloids [6], and even millimeter-sized charged or magnetized beads [7–9]. Moreover, a fluctuation applied by the tuning temperature, strength of the interaction, or artificial agitation can induce melting transition of these confined solid phases [6,8,10]. The configurations of confined interacting particles and their phase transitions were extensively studied through numerical simulations [11,12].

Among them, vortices in mesoscopic-scale superconductors have been investigated extensively in the past two decades. As the confinement effect of a screening current circulating along the edges is relatively stronger in smaller superconductors, unique vortex arrangements, e.g., giant vortex, symmetrically induced antivortex, and shell structures, were expected to be formed in microfabricated thin films of conventional superconductors [1,13–15]. Particularly, shell structures were observed in rather larger disk-shaped samples and directly visualized through the Bitter decoration method [1] or a scanning superconducting quantum interference device microscope [16]. Moreover, there are studies on vortex configurations in other shapes such as equilateral triangles, squares, and pentagons [17–22]. Although it is interesting to determine whether the evolution of the configuration with the addition of vortices and stable (magic) numbers of vortices are thoroughly explained by the concept of "shell," the definition of shell itself is not always decisive if the number of vortices N is quite large or if the sample shape is far from a disk, especially a triangle [20,23].

The stability of spatial configurations influences thermodynamic quantities such as melting temperature. Because the first-order melting transition of a vortex solid to a liquid is observed in bulk crystals of $Bi_2Sr_2CaCu_2O_{8+y}$ (Bi2212) high-T_c superconductors in easily accessible field ranges [24], microfabricated Bi2212 crystals can be utilized to study the melting transition of confined vortex crystals or clusters, which would demonstrate the stability and evolution of vortex configurations with an increase in N. We have reported an oscillating behavior of the melting transition line in square-shaped Bi2212 single crystals of lateral size μm through c-axis magnetoresistance measurements using a stack of intrinsic Josephson junctions (IJJs) [25]. The oscillating part of the melting temperature was at a broad maximum around the number of vortices $N = n^2$ (n is an integer number), suggesting that the vortex states containing a square number of vortices are stabilized owing to geometrical matching of confined vortex crystals and the square boundary shape. However, in the case of the square, frustration with respect to the symmetries between the square boundary and vortex lattice, which prefer to form a hexagonal lattice in an infinite
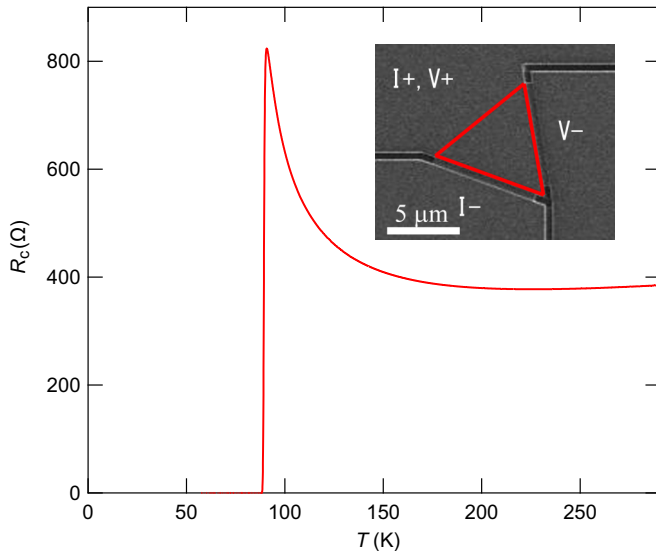
FIG. 1. Temperature dependence of c-axis resistance R_c for a fabricated triangle-shaped stack of Bi2212 IJJs. Inset: SIM image of the same sample (top view). Three Bi2212 electrodes are extended from the top or bottom of the stack.

bulk, makes the problem of the stabilities of N-vortex states complex. Therefore, the use of triangle-shaped samples can mitigate this problem.

In this paper, we present experimental results of the melting transition of vortex crystals (or clusters) confined in a triangle-shaped mesoscopic Bi2212. The oscillating behavior of melting temperatures is confirmed in the triangle as well as in the squares. By comparing with numerical calculations for the configurations of N-vortex states, we conclude that the two-dimensional geometrical matching of hexagonal vortex crystals in the triangle shape is realized at the triangular number $N = n(n + 1)/2$, whereas suppression of melting temperatures in nonmatching states is mainly caused by geometrically induced defect structures, which are edge dislocations in many cases.

II. EXPERIMENTS

High-quality single crystals of Bi2212 were grown using the traveling-solvent floating-zone method [26]. A triangle-shaped stack of IJJs was fabricated via a double-sided etching process using a focused ion beam (FIB) without adhesives, which is very similar to the method proposed by Latyshev *et al.*, in which narrow trenches were formed on the top and bottom surfaces using FIB by a flipping of whiskers [27]. The only difference from their method is the shape of the starting crystal; a cleaved flake of single crystal was used instead of whiskers. In addition, parts of electrodes were fabricated by separating each Bi2212 electrode using FIB milling. A scanning ion microscope (SIM) image of the triangular stack sample is shown in the inset of Fig. 1. An electrode for current and another for voltage are directly placed at the bottom of the stack, and a top electrode is commonly used for current and voltage. The length l of the side of the equilateral triangular stack is ∼8 μm, and the thickness of the stack is ∼100 nm, which is estimated from room-temperature resistance using
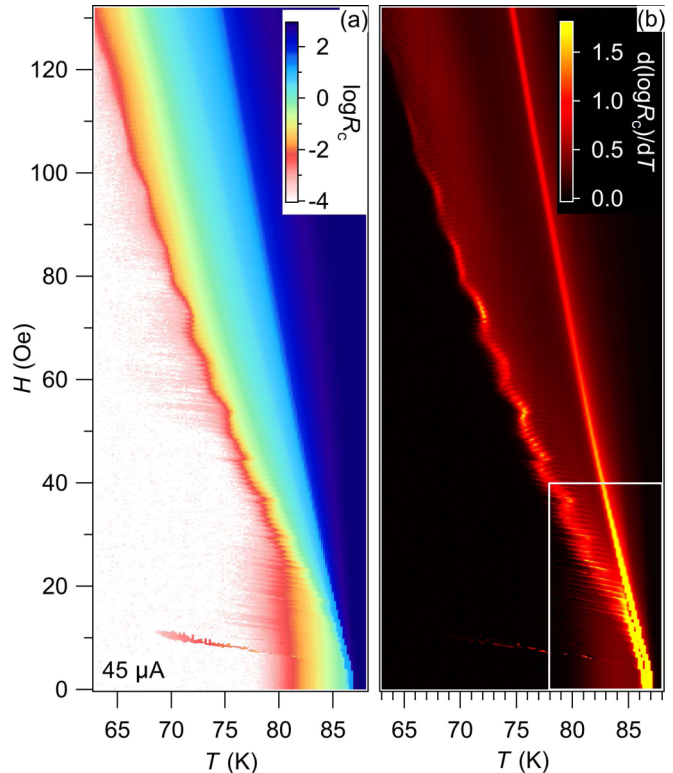

FIG. 2. Color maps of (a) $\log R_c$ and (b) $d \log R_c / dT$ on H-T planes for the triangular sample of Bi2212. The applied current is 45 μA.

the typical Bi2212 c-axis resistivity of 10 Ω cm. The c-axis resistance R_c was measured using a current source (Keithley 6430) and a nanovoltmeter (Keithley 2182) in a chamber containing a sample stage cooled by a Solvay-type cryocooler. As shown in Fig. 1, R_c shows typical up-turn behavior in the normal state. The superconducting transition temperature was 89 K at the midpoint of the resistance drop. A magnetic field was applied parallel to the c axis of Bi2212, i.e., normal to the image in Fig. 1. All the data of R_c were acquired through repeated field scans from negative to positive at various fixed temperatures.

III. EXPERIMENTAL RESULTS

To reveal the phase diagram of vortices confined in the triangular sample, we repeatedly measured R_c as a function of magnetic field with an applied current of 45 μA at a fixed temperature, which was changed from 63 to 88 K in increments of 0.1 K. It is possible to detect the melting transition by the R_c measurements as a steep increase of R_c with increasing temperature or magnetic field [28,29]. Since the melting of the vortex lattice in Bi2212 is accompanied by a decoupling of pancake vortices along the c axis [30,31], flow of Josephson vortices connecting the misaligned pancake vortices in the liquid phase can bring about the increase of R_c.

Figures 2(a) and 2(b) show color maps of $\log R_c$ and its temperature differentiation $d \log R_c / dT$ on an H-T plane, respectively. Note that $d \log R_c / dT$ represents $d \log(R_c + \delta R)/dT$, in which a small offset δR was added to R_c. This is the same procedure as that used in our previous study to
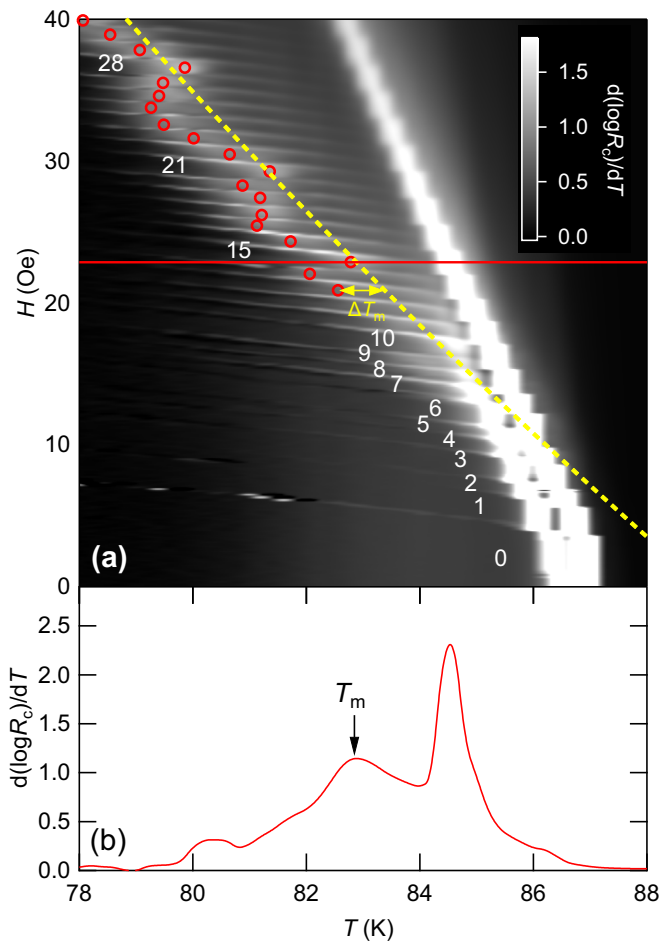
FIG. 3. (a) Zoomed-in map of $d \log R_c/dT$ in a gray scale, which is the part of the white box in Fig. 2(b). The number of vortices N obtained by counting the number of slash lines from the zero field is shown for some N in the regions between the slashes. T_m is extracted from the points of the red circles. The yellow dashed line is calculated from the decoupling theory (see the main text), which is used as a smooth background $T_{BG}(H)$ to extract the oscillating part of T_m, i.e., $\Delta T_m = T_m - T_{BG}$. The definition of ΔT_m is also illustrated by a yellow arrow. (b) Line profile of $d \log R_c/dT$ on the red line in (a).
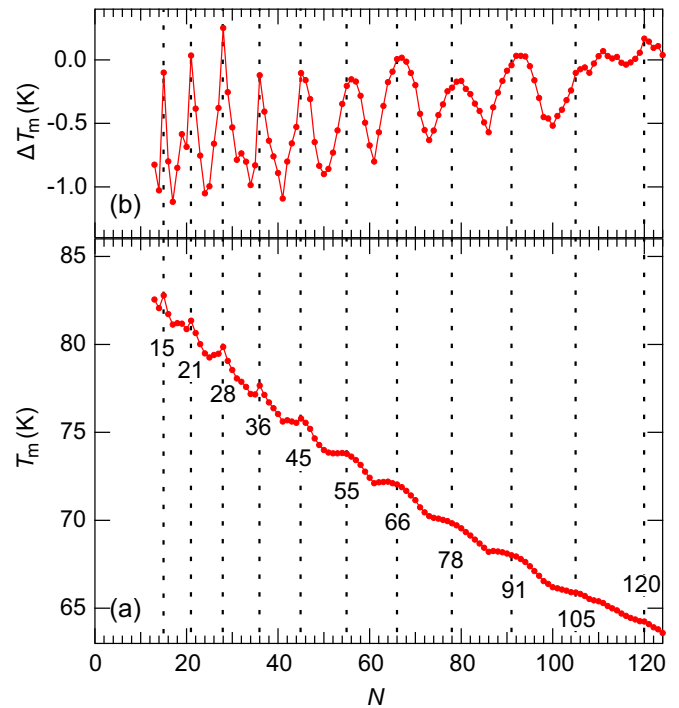

FIG. 4. (a) Vortex-number dependence of the melting transition temperature $T_m(N)$. T_m for $N < 13$ is not plotted because the melting line is not well determined in Fig. 2(b) or Fig. 3(a) owing to the limitation of the critical current of IJJs. (b) Vortex-number dependence of ΔT_m, i.e., the oscillating part of $T_m(N)$, whose definition is shown in the main text and the caption of Fig. 3.

reduce noise in $d \log R_c/dT$ in the zero-resistance region [25]. A steep increase in $\log R_c$ with an increase in the temperature is represented by a peak in $d \log R_c/dT$, corresponding to bright colors from red to yellow in Fig. 2(b). The three features observed in squared Bi2212 [25] are also reproduced in this triangular Bi2212: (1) an upper bright line from the top center to the bottom right, indicating that the critical current of IJJs becomes smaller than the applied current at this point, (2) an oscillating bright line below the first line, corresponding to the melting transition line of vortex crystals, and (3) almost equally separated fine horizontal slashes caused by each vortex entry into the sample, particularly clear around the melting line in lower fields.

The first feature is extrinsic because it strongly depends on the applied current. We extracted the melting temperatures T_m and fields H_m from the oscillating line of the second feature. The extracted melting points at low fields are shown by red

circles in a zoomed-in $d \log R_c/dT$ map of Fig. 3(a). Figure 3(b) shows a line profile of $d \log R_c/dT$ in 23 Oe, where the melting transition is observed as a peak. The number of vortices involved in the melting transition is determined by counting the number of slashes from the lowest one, whose details can be seen in Fig. 3(a).

The vortex-number dependence of the melting transition temperature is plotted with vertical grids indicating triangular numbers $N_{tri} = n(n+1)/2$ in Fig. 4(a). Clear enhancements of T_m at the triangular numbers are observed as sharp peaks for smaller vortex numbers, whereas they become broad maxima above $N \sim 50$. Figure 4(b) shows an oscillating component of T_m (ΔT_m), which is evaluated by subtracting a background curve expressed by $T_{BG}(H) = T_c(H_0/(H_0 + H))$ of the decoupling theory [32], where $H_0 = 310$ Oe and $T_c = 89.0$ K. The amplitude of the oscillations reaches approximately 1 K at lower N, whereas it gradually decreases with an increase in N. Between the maxima of the oscillations, dips are also well defined even when the peak becomes broad at larger numbers. Similar dip structures were also observed in the case of the squared Bi2212, where the dips are much sharper than the broad peaks for the entire N [25], although the reason is still unclear.

From the intervals between the nearest-neighbor slash lines, we can evaluate the field range ΔH of the N-vortex state, where the number of vortices is maintained. Since changes of ΔH were very small especially at higher fields, to increase the resolution $R_c(H)$ measurements with much
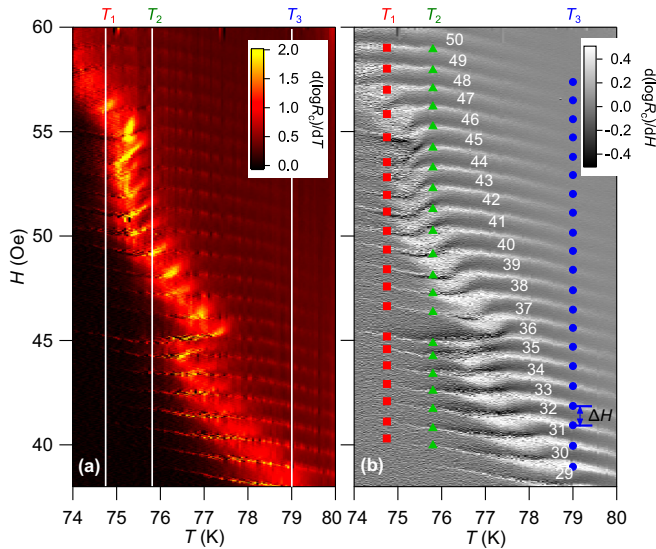
FIG. 5. Details of (a) $d \log R_c/dT$ and (b) $d \log R_c/dH$ maps in an intermediate field range. ΔH are extracted at three temperatures: $T_1 = 74.75$, $T_2 = 75.8$, and $T_3 = 79.0$ K. In (b), the color markers indicate the positions of the slash lines at each temperature, which are used to evaluate ΔH. The number of vortices N and an example of the definition of ΔH are also shown.

FIG. 6. Vortex-number dependence of field range ΔH at three different temperatures [(a)–(c)]. The two vertical grids show the triangular numbers of 36 and 45, respectively.

finer steps of temperature and field were conducted in an intermediate field range. The obtained maps of $d \log R_c/dT$ and $d \log R_c/dH$ are shown in Fig. 5(a) and 5(b), respectively. It is more convenient to use the field-derivative map to count the number of vortices, because it makes the slash lines clearer, compared with the temperature-derivative map. ΔH are extracted from Fig. 5(b), and Fig. 5(a) is used to evaluate the melting transition line.

In Fig. 6, ΔH as a function of N is plotted at three temperatures labeled by T_1, T_2, and T_3 in Fig. 5. As shown in Fig. 6(a), ΔH is nonuniform in vortex solid phase ($N < 48$). Particularly, significant enhancements are observed at N_{tri} of 36 and 45. While the same feature can also be observed in the solid phase ($N < 41$) in Fig. 6(b) for a slightly higher temperature, ΔH becomes almost constant in the liquid phase [$N \geqslant 41$ in Fig. 6(b) and $N \geqslant 29$ in Fig. 6(c)]. In the simulations by Cabral *et al.*, it is expected that ΔH reflects the stability of vortex configuration at each N and is enhanced at the triangular numbers [23]. Our findings experimentally confirm that the configuration of vortex crystals at N_{tri} is more stable than those at the other numbers, which is consistent with the aforementioned simulations [23]. As mentioned in Ref. [23], the configurations at N_{tri} are analogous to the "noble gas." Moreover, in their simulations, excess suppression of ΔH was observed in the "halogen" states of $N_{\mathrm{tri}} - 1$, which is also observed in Fig. 6 ($N = 35$ and 44). Contrary to the solid state, the liquid state of each N does not have a distinct difference in ΔH, suggesting its homogeneous nature.

IV. NUMERICALLY SIMULATED VORTEX CONFIGURATIONS

Vortex configurations in an equilateral-triangle mesoscopic superconductor have already been investigated theoretically
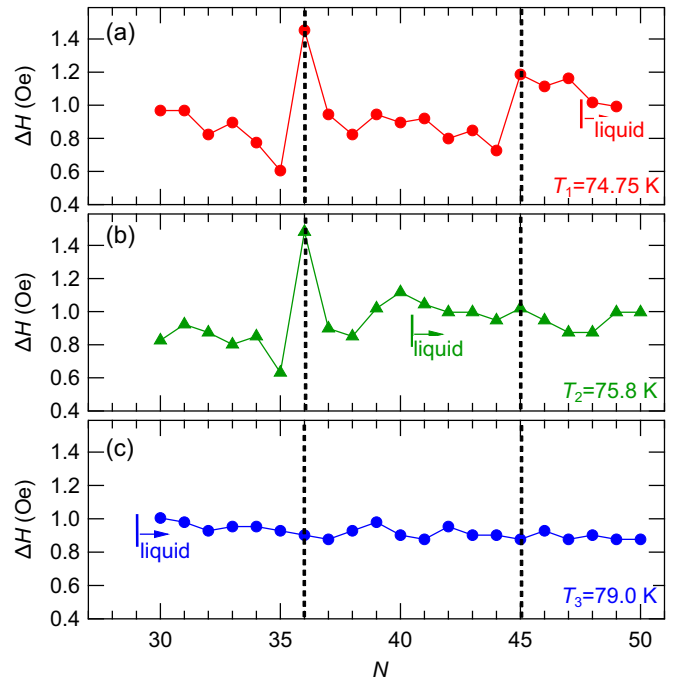
based on the London or Ginzburg-Landau (GL) approach for a limited number of vortices [17,23,33–35]. Cabral *et al.* calculated the ground-state configurations up to $N = 37$ in the simulations and tried to classify them [23]. To compare our experimental results with theoretical configurations for larger numbers of vortices, we numerically calculated configurations with the number of vortices more than 60. Vortex entries into an equilateral superconducting triangle were simulated using the GL equations with the finite element method (COM-SOL Multiphysics®[36]), according to the procedures and implementations of time-dependent GL equations developed by Alstrøem *et al.* [37]. Solutions of steady states were obtained for each dimensionless magnetic field B_a with its parametrical increments. In our simulations, to reduce the number of meshes and the calculation time, the GL parameter κ was set to 10, which is sufficient to determine the vortex configurations, whereas it is known to be $\sim$100 in high-T_c cuprate superconductors. The length l of a side of the triangle was fixed to 10 times of the penetration depth λ, which is not significantly different from the size of our sample. The resultant configurations almost reproduced the previous studies in the London limit [23], although thermodynamic quantities, i.e., free energy or magnetization, show a hysteretic behavior in our calculations depending on the field-sweep process owing to the Bean–Livingston barrier [38]. To avoid multivortex entries at once, a tiny notch is introduced on one side, which promotes one-by-one vortex entries.

The obtained configurations were analyzed using Delaunay triangulation to identify the locations of topological defects. The coordination number n_i of a vortex i is defined as the number of bonds connected to it in the triangulated configuration. In the case of an Abrikosov hexagonal lattice, n_i is 6 for
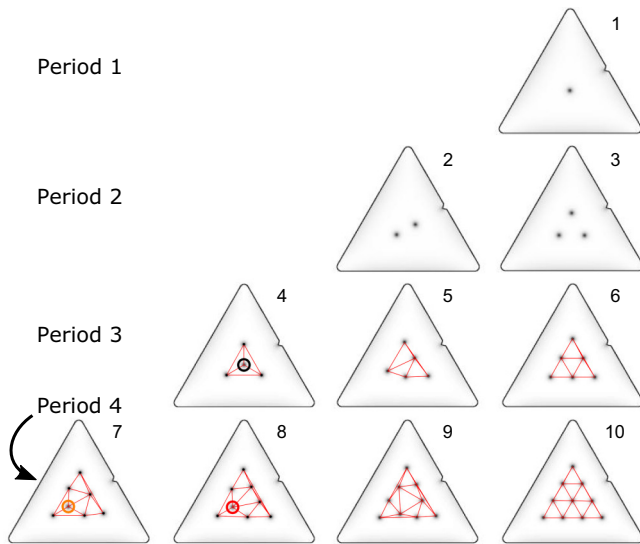
FIG. 7. Calculated vortex configurations from $N = 1$ to 10. Geometrical matching realized at the triangular numbers $N_{tri} = 1, 3, 6,$ ..., $n(n + 1)/2$ (n is an integer). Resembling the periodic table of elements, the evolution of the configuration with vortex number has a periodicity and is arranged in terms of N_{tri} in the present case. In each row, the configuration at the right end of N_{tri} corresponds to the "noble gas" state.

vortices in bulk and n_i is 4 for vortices on straight boundaries. Therefore, a vortex with $n_i \neq 6$ is considered as a topological defect in bulk. The charge of topological defects is defined by $Q_i \equiv 6 - n_i$ in bulk and $Q_i \equiv 4 - n_i$ on the boundary. In this study, topological defects in bulk with $Q_i = 3, 2, 1,$ and -1 are marked by black, orange, red, and blue circles, respectively, in Figs. 7–9. Optionally, those located close to boundaries are marked by dotted circles if necessary. The summation of the charges for all vortices is 6, i.e., $\sum_i Q_i = 6$ owing to Euler's
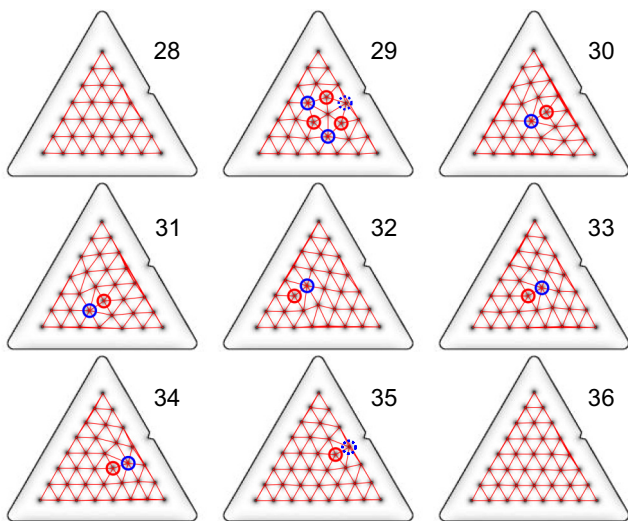

FIG. 8. Simulated vortex configurations for a matching number of $N = 28$ and for the eighth period, i.e., from $N = 29$ to 36. At the nonmatching numbers except $N = 29$, the defect structures are edge dislocations, which are indicated by the pairs of red and blue circles.
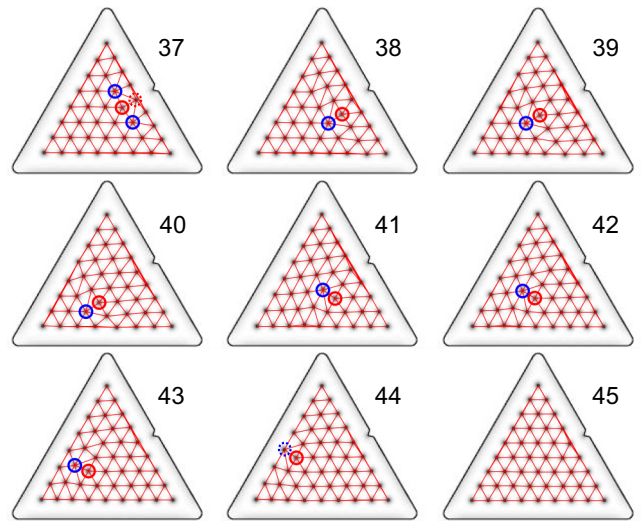

FIG. 9. Simulated vortex configurations for the ninth period. Similar to Fig. 8, in most cases, the observed defect in the nonmatching state is an edge dislocation.

polyhedron theorem. An adjacent pair of $+1$ and -1 charges corresponds to an edge dislocation.

Figure 7 shows the obtained configurations for $N = 1$ to 10. To clarify the periodicity with N_{tri}, the configurations at N_{tri} are arranged along the rightmost column, like noble gases in the periodic table of elements. In this arrangement, we refer to the first row as the first period,..., and the nth row as the nth period. Only the configuration for $N = 9$ is different from the ground state obtained by Cabral *et al.*, but it is the same as one of two metastable states obtained by them [23].

For $N = 11$ to 36, our configurations are the same as the results obtained by Cabral in many cases except for $N = 14,$ 23, 24, 27, 29–32. Particularly, the configurations at N_{tri} of 15, 21, 28, and 36 are Abrikosov hexagonal lattices in both cases. It appears trivial that perfect geometrical matching occurs at N_{tri}, because the symmetry of the hexagonal lattice coincides with that of the equilateral triangle. Our simulations provide the perfect hexagonal lattice up to 45 (the ninth triangular number), but fail at 55 (the tenth triangular number). Vortex configurations from $N = 28$ to 36 and from 37 to 45 are shown in Figs. 8 and 9, respectively.

V. DISCUSSION

In our simulations, particularly with larger number of vortices, we observed an interesting evolution in the configurations where the nonmatching states contain an edge dislocation in many cases and only the positions of the dislocations differ with the change in N. This is observable in the eighth and ninth periods as shown in Figs. 8 and 9, respectively. With an increase in N from N_{tri}, excess vortices induce defect structures. Except for $N = N_{tri} + 1$, the defect is identical to an edge dislocation, and the position changes for different N. When N is one before the next N_{tri}, the edge dislocation appears on a boundary, and then disappears at the next N_{tri}. Hence, it is most likely that the periodical appearance of an edge dislocation between N_{tri} causes the oscillations of the melting transition temperature.

Suppression of the melting field or temperature by the introduction of a geometrically induced dislocation is roughly estimated as follows. The energy of an elementary edge dislocation in the vortex lattice is $db^2 c_{66}/2\pi \ln(R_s/R_0)$, where d is the thickness, b is the Burgers vector, c_{66} is the shear modulus, and R_s, R_0 are the sample and dislocation core radii, respectively [39]. c_{66} is approximately $\Phi_0 B/(8\pi\lambda)^2$. As the Burgers vector and the core radius are expected to be comparable to lattice spacing a_0 (for hexagonal lattice, $a_0^2 = 2\Phi_0/\sqrt{3}B$), the dislocation energy per unit volume e_{dis} can be expressed by

$$e_{\text{dis}} = \frac{\varepsilon_0}{4\sqrt{3}\pi S} \ln\left(\frac{R_s}{a_0}\right), \tag{1}$$

where $\varepsilon_0 = (\Phi_0/4\pi\lambda)^2$ is the basic energy scale of vortex system and S is the sample area. To estimate the suppression of melting temperature by the introduction of an edge dislocation, we consider a case where a dislocation-free vortex configuration with N vortices in an arbitrary sample shape is modified to a configuration with an edge dislocation for the same N by transforming the sample shape to a triangle. If the melting field H_{m0} of the dislocation-free configuration is reduced to $H_{m0} - \delta H$ by the introduction of the dislocation at a fixed temperature, the free energy of the crystal and liquid states in both cases fulfills

$$g_{\text{cr}}(H_{m0}) = g_l(H_{m0}), \tag{2}$$

$$g_{\text{cr}}^{\text{dis}}(H_{m0} - \delta H) = g_l(H_{m0} - \delta H), \tag{3}$$

at the melting point. Expanding Eq. (3) to the first order in δH,

$$g_{\text{cr}}^{\text{dis}}(H_{m0}) - g_l(H_{m0}) \simeq \left(\frac{\partial g_{\text{cr}}^{\text{dis}}}{\partial H}\bigg|_{H_{m0}} - \frac{\partial g_l}{\partial H}\bigg|_{H_{m0}} \right) \delta H \tag{4}$$

$$= -\frac{1}{4\pi}\left(B_{\text{cr}}^{\text{dis}} - B_l\right)\delta H. \tag{5}$$

Assuming that the magnetization jump of the melting transition $B_{\text{cr}}^{\text{dis}} - B_l$ for the configuration with a dislocation does not change considerably from the value observed in bulk crystals $(-\Delta B)$, the enhancement of free energy by the introduction of a dislocation is given by $g_{\text{cr}}^{\text{dis}} - g_{\text{cr}} \sim (\Delta B/4\pi)\delta H$. Using Eq. (1) for the energy of the dislocation, we obtain

$$\delta H = \frac{\varepsilon_0(T)}{\sqrt{3}S\Delta B} \ln\left(\frac{R_s}{a_0}\right). \tag{6}$$

For $S = 27.7$ μm^2, $\lambda \sim 700$ nm at 75 K, $\Delta B = 0.1$ G, and $\ln(R/a_0) \sim 1$, δH is estimated to be 1.2 Oe. Using $dT_m/dH \sim 0.2$ [K/Oe] as a slope of the melting transition line, the expected suppression of the melting temperature is 0.24 K, whose order is comparable to the experimental result in Fig. 4. Therefore, it is highly possible that the emergence of an edge dislocation induced by the geometrical confinement is the origin of the melting-temperature suppression in the nonmatching states.

Although Eq. (6) indicates an increase in the oscillation amplitude at higher fields and lower temperatures, the experimental results appear contrary and the oscillations almost disappear above $N > 100$ as shown in Fig. 4. There is a possibility that unintended imperfections of the sample such as accuracy of the equilateral triangle or bulk pinning by quenched disorder smear the geometrical matching phenomena, particularly for large N. Nevertheless, as our estimation only considers the energy of an edge dislocation and does not consider the entire influence of the screening current, more precise calculations may resolve this discrepancy.

In conclusion, to reveal the influence of confinement effect on the melting transition of vortex crystals or clusters, we have investigated the melting transition in a μm-sized triangle of the superconducting Bi2212 single crystal using c-axis magnetoresistance measurements with a stack of IJJs. As in the case of the square samples, an oscillating behavior of the melting transition line was observed in the triangle. Sharp peaks of the melting temperatures appear at the triangular numbers of vortex $N = n(n+1)/2$, at least for $N < 50$. Two-dimensional geometrical matching of the hexagonal vortex crystal with the triangle shape is the origin of the peaks. Through a comparison with our numerical studies on the vortex configuration for each N, it is observed that suppression of the melting temperature in the nonmatching states mainly originates from defect structures such as edge dislocations. Further studies with different sample shapes or by using other experimental methods such as direct vortex imaging or thermodynamic magnetization measurement would allow a deeper insight into the melting phenomenon in confined vortex crystals.

[1] I. V. Grigorieva, W. Escoffier, J. Richardson, L. Y. Vinnikov, S. Dubonos, and V. Oboznov, Phys. Rev. Lett. **96**, 077005 (2006).

[2] E. J. Yarmchuk, M. J. V. Gordon, and R. E. Packard, Phys. Rev. Lett. **43**, 214 (1979).

[3] K. W. Madison, F. Chevy, W. Wohlleben, and J. Dalibard, Phys. Rev. Lett. **84**, 806 (2000).

[4] J. R. Abo-Shaeer, C. Raman, J. M. Vogels, and W. Ketterle, Science **292**, 476 (2001).

[5] W.-T. Juan, Z.-H. Huang, J.-W. Hsu, Y.-J. Lai, and L. I, Phys. Rev. E **58**, R6947(R) (1998).

[6] R. Bubeck, C. Bechinger, S. Neser, and P. Leiderer, Phys. Rev. Lett. **82**, 3364 (1999).

[7] M. S. Jean, C. Even, and C. Guthmann, Europhys. Lett. **55**, 45 (2001).

[8] J. Schockmel, E. Mersch, N. Vandewalle, and G. Lumay, Phys. Rev. E **87**, 062201 (2013).

[9] J. Schockmel, N. Vandewalle, E. Opsomer, and G. Lumay, Phys. Rev. E **95**, 062120 (2017).

[10] A. Melzer, A. Schella, J. Schablinski, D. Block, and A. Piel, Phys. Rev. Lett. **108**, 225001 (2012).

[11] V. M. Bedanov and F. M. Peeters, Phys. Rev. B **49**, 2667 (1994).

[12] E. Yurtsever, F. Calvo, and D. J. Wales, Phys. Rev. E **72**, 026110 (2005).

[13] A. K. Geim, I. V. Grigorieva, S. V. Dubonos, J. G. S. Lok, J. C. Maan, A. E. Filippov, and F. M. Peeters, Nature **390**, 259 (1997).

[14] T. Cren, L. Serrier-Garcia, F. Debontridder, and D. Roditchev, Phys. Rev. Lett. **107**, 097202 (2011).

[15] L. F. Chibotaru, A. Ceulemans, V. Bruyndoncx, and V. V. Moshchalkov, Nature **408**, 833 (2000).

[16] N. Kokubo, S. Okayasu, A. Kanda, and B. Shinozaki, Phys. Rev. B **82**, 014501 (2010).

[17] H. J. Zhao, V. R. Misko, F. M. Peeters, S. Dubonos, V. Oboznov, and I. V. Grigorieva, Europhys. Lett. **83**, 17008 (2008).

[18] H. J. Zhao, V. R. Misko, F. M. Peeters, V. Oboznov, S. V. Dubonos, and I. V. Grigorieva, Phys. Rev. B **78**, 104517 (2008).

[19] N. Kokubo, S. Okayasu, T. Nojima, H. Tamochi, and B. Shinozaki, J. Phys. Soc. Jpn. **83**, 083704 (2014).

[20] N. Kokubo, H. Miyahara, S. Okayasu, and T. Nojima, J. Phys. Soc. Jpn. **84**, 043704 (2015).

[21] P. J. Pereira, V. V. Moshchalkov, and L. F. Chibotaru, Phys. Rev. E **86**, 056709 (2012).

[22] H. T. Huy, M. Kato, and T. Ishida, Supercond. Sci. Technol. **26**, 065001 (2013).

[23] L. R. E. Cabral and J. A. Aguiar, Phys. Rev. B **80**, 214533 (2009).

[24] E. Zeldov, D. Majer, M. Konczykowski, V. B. Geshkenbein, V. M. Vinokur, and H. Shtrikman, Nature **375**, 373 (1995).

[25] S. Ooi, T. Mochiku, M. Tachiki, and K. Hirata, Phys. Rev. Lett. **114**, 087001 (2015).

[26] T. Mochiku, K. Hirata, and K. Kadowaki, Physica C **282-287**, 475 (1997).

[27] Y. I. Latyshev *et al.*, JETP Lett. **69**, 84 (1999).

[28] D. T. Fuchs, R. A. Doyle, E. Zeldov, D. Majer, W. S. Seow, R. J. Drost, T. Tamegai, S. Ooi, M. Konczykowski, and P. H. Kes, Phys. Rev. B **55**, R6156(R) (1997).

[29] S. Ooi, S. Savel'ev, M. Gaifullin, T. Mochiku, K. Hirata, and F. Nori, Phys. Rev. Lett. **99**, 207003 (2007).

[30] T. Shibauchi, T. Nakano, M. Sato, T. Kisu, N. Kameda, N. Okuda, S. Ooi, and T. Tamegai, Phys. Rev. Lett. **83**, 1010 (1999).

[31] M. B. Gaifullin, Y. Matsuda, N. Chikumoto, J. Shimoyama, and K. Kishio, Phys. Rev. Lett. **84**, 2945 (2000).

[32] L. I. Glazman and A. E. Koshelev, Phys. Rev. B **43**, 2835 (1991).

[33] L. F. Chibotaru, A. Ceulemans, V. Bruyndoncx, and V. V. Moshchalkov, Phys. Rev. Lett. **86**, 1323 (2001).

[34] B. J. Baelus and F. M. Peeters, Phys. Rev. B **65**, 104515 (2002).

[35] L. R. E. Cabral, J. Barba-Ortega, C. C. de Souza Silva, and J. Albino Aguiar, Physica C **470**, 786 (2010).

[36] COMSOL Multiphysics®www.comsol.com, COMSOL AB, Stockholm, Sweden.

[37] T. S. Alstrøm, M. P. Sørensen, N. F. Pedersen, and S. Madsen, Acta Appl. Math. **115**, 63 (2010).

[38] C. Bean and J. Livingston, Phys. Rev. Lett. **12**, 14 (1964).

[39] G. Blatter and V. B. Geshkenbein, in *Superconductivity*, edited by K. H. Bennemann and J. B. Ketterson (Springer, Berlin, Heidelberg, 2008), Chap. 12, pp. 495–637.